

## Optical closure in lakes with contrasting extremes of reflectance

C. L. Gallegos<sup>1</sup>

Smithsonian Environmental Research Center, P.O. Box 28, Edgewater, Maryland 21037

R. J. Davies-Colley

National Institute of Water and Atmospheric Research, Box 11-115, Hamilton, New Zealand

M. Gall

National Institute of Water and Atmospheric Research, P.O. Box 8602, Riccarton, Christchurch, New Zealand

### *Abstract*

We measured inherent and apparent optical properties and computed ‘optical closure’ in four lakes on the South Island of New Zealand, ranging very widely in reflectance. Optical properties were measured by modern instruments deployed from boats, with supporting laboratory measurements on water samples. The radiative transfer model, Hydrolight, was used with measured inherent optical properties to predict characteristics of the light field for comparison with field measurements. Two glacier-fed lakes were strongly light-scattering and weakly light-absorbing, with optical properties dominated by glacial flour. In marked contrast, two humic-stained wetland lakes were strongly light-absorbing and weakly light-scattering, with optical properties dominated by colored dissolved organic matter. Very good optical ‘closure’ (i.e., agreement of modeled with measured characteristics of the light field) was obtained for all apparent optical properties examined in all but the most strongly light-scattering lake. Closure was achieved when systematic spectral bias in absorption in this lake, possibly caused by multiple scattering in the field absorption meter, was corrected using laboratory absorption measurements. The highest and lowest measured and modeled water-leaving radiances exceeded the previous range for such studies by a factor of 5. The good optical closure observed over a very wide (200-fold) range of reflectance increases confidence in our ability to specify inputs for radiative transfer modeling while highlighting the enduring challenge of accurately measuring absorption in highly scattering waters and backscattering in highly absorbing waters.

Optical ‘closure’ refers to the testing of theoretical interrelationships between measured inherent optical properties (IOPs, characteristics of the water) and apparent optical properties (AOPs, characteristics of the in situ light field) of a water body (Zaneveld 1994). Demonstration of optical closure can increase confidence in theoretical relationships derived from radiative transfer (RT) modeling (Zaneveld 1994), while failure to obtain agreement between modeled and measured quantities can reveal critical uncertainties and sensitivities in measured data (Bulgarelli et al. 2003). Demonstration of closure is an important step in the derivation of remote sensing algorithms, lending confidence in the derived relationships (Chang et al. 2003;

Tzortziou et al. 2006, 2007). Closure depends on obtaining accurate measurements of the IOPs of the water body, which are used as input to an RT model, along with relevant environmental conditions (solar altitude, cloud cover, water surface conditions, depth, and bottom albedo) to predict measurable attributes of the underwater light field, from which the emergent light field can be estimated (Tzortziou et al. 2006).

The IOPs of a water body are completely specified by the spectral absorption coefficient ( $a$ ) and spectral volume scattering function (VSF; Mobley 1994). AOPs of interest include spectral irradiance attenuation coefficients and spectral remote sensing reflectance. Advances in instrumentation for measuring IOPs and AOPs in the last decade have made possible the demonstration of optical closure in several coastal oceanic waters, including the northern Adriatic (Bulgarelli et al. 2003), coastal New Jersey (Chang et al. 2003), and Chesapeake Bay (Tzortziou et al. 2006). These are all examples of optically complex (known as ‘Case 2’) waters, in which concentrations of light-attenuating substances (LAS), primarily colored dissolved organic matter (CDOM), phytoplankton, detritus, and mineral sediment, tend to vary independently as a result of terrestrial inputs and local resuspension of particulate matter. (In optically simpler ‘Case 1’ waters, which are usually remote from land, optical properties vary systematically with phytoplankton biomass [Morel 1988].)

Independence among concentrations of LAS presents severe challenges in terms of developing remote sensing algorithms for estimating water composition. River plumes

<sup>1</sup> Corresponding author (gallegosc@si.edu).

### *Acknowledgments*

We thank Ian Halstead and Doug Griffin of the National Institute of Water and Atmospheric Research (NIWA) field stations (at Tekapo and Greymouth, respectively) for field assistance and logistical support. Ron Ovenden (NIWA-Hamilton) conducted a particle size analysis, and scanning electron micrographs were kindly prepared by Cathy Kilroy, NIWA-Christchurch, using the Canterbury University electron microscopy facility. We also thank E. Amy Lewis (Smithsonian Environmental Research Center) for help with data processing and Sanjay Wahdwa (NIWA-Hamilton) for the location map (Fig. 1). The manuscript was appreciably improved in response to review comments by Dariusz Stramski and two reviewers.

Funding was provided by NIWA (Clive Howard-Williams) through the New Zealand Foundation for Research, Science and Technology (FRST) Capability Fund, Contract CVSM062.

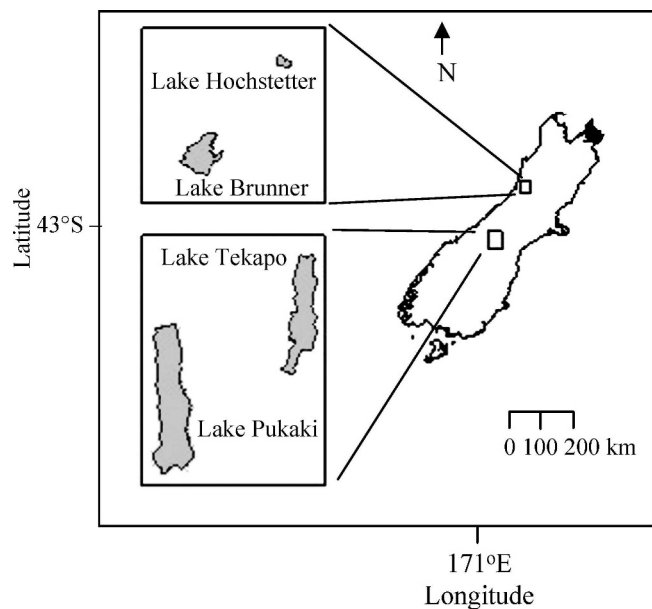


Fig. 1. Location of lakes studied on the South Island of New Zealand. Lakes Hochstetter and Brunner are located on the west (perhumid) side of the Southern Alps and are dominated by colored dissolved organic matter. Lakes Tekapo and Pukaki are located on the east side of the Southern Alps (in their rain-shadow, with prevailing westerly winds) and are dominated by glacial flour.

and sediment resuspension by wind-waves in shallow waters add CDOM and nonalgal particulates (NAP) in varying amounts and proportions, and with optical properties specific to the particular sources. For example, rivers delivering suspended sediments from agricultural areas may affect coastal optical properties differently from glacier-fed streams as a result of differences in mineralogy, organic content, and particle-size distribution (Babin et al. 2003; Babin and Stramski 2004). Consequently, remote sensing algorithms and parameterizations for Case 2 waters tend to be highly localized (Magnuson et al. 2004).

In deriving local algorithms it is an advantage to know the optical properties of LAS from proximal sources in isolation. Such knowledge is a prerequisite for accurate prediction of coastal optical properties from physical transport and optical modeling. Inland waters (i.e., lakes

and rivers) provide a valuable opportunity to examine the optical properties of primary source material prior to mixing with coastal waters. Furthermore, inland waters are probably more optically extreme than coastal waters (Davies-Colley et al. 2003), in terms of reflectance, for example, thus providing more severe tests of optical measurement and modeling capability. The aim of this work was to characterize the optical properties and to test optical closure in lakes that are extreme in both their domination by LAS other than phytoplankton and their resulting reflectance. We measured IOPs and AOPs and computed optical closure in two highly reflective, glacier-fed lakes and in two markedly contrasting (low-reflectance) lakes dominated by CDOM, in one field campaign using the same suite of instruments. The optics of such systems are important in the context of a changing global climate, as increased melting of glaciers carries the short-term potential to deliver greater concentrations of highly reflective particulate matter to coastal waters; and changing rainfall patterns interacting with land-use transformations (e.g., wetlands drainage, reduced soil permeability) may alter the delivery of sediment and CDOM to coasts in ways that are difficult to predict. Our study is noteworthy for applying closure tests to waters that are both brighter and darker than those in which this practice has previously been attempted.

## Methods

*Study sites*—We measured IOPs and AOPs at central stations in four lakes in South Island, New Zealand (Fig. 1; Table 1), in February (the southern summer) 2006. Lakes Pukaki and Tekapo (names given by indigenous Maori people) occupy glacial troughs located in the MacKenzie District in the rain shadow (east) of the Southern Alps and are fed by glacial meltwater rivers, the Tasman and Godley Rivers, respectively. These high-gradient, short-transit-time rivers have cold water and little interaction with vegetated terrain, and consequently the lakes are ultra-oligotrophic, very low in CDOM, and have optical properties dominated by inorganic suspensoids (‘glacial flour’) (Vant and Davies-Colley 1984). The lakes are notable for their bright turquoise color and very high reflectance (Davies-Colley et al. 2003). The geology of the glaciated subcatchments in the Pukaki Catchment is mainly

Table 1. Sampling dates, location of stations, and water quality concentrations observations and measurements in water samples collected during an optical measurement campaign in four South Island, New Zealand lakes (February 2006). \* Munsell color is hue code observed through an underwater viewer. Numbers (e.g., 57.5) are hue numbers on the (continuous) Munsell hue scale, and letter codes (in parentheses) are as follows: BG, blue-green; Y, yellow; YR, yellow-red (orange).

Lake	Date	Latitude	Longitude	$Z_{eu}$ (m)	Munsell hue number (code)	$a_g(440)$ ( $m^{-1}$ )	Chl <i>a</i> ( $mg\ m^{-3}$ )	TSS (%organic) ( $g\ m^{-3}$ )	$b_p(555)$ :TSS ( $m^2\ g^{-1}$ )
Pukaki	07 Feb 06	-44.097	170.203	5	57.5(7.5BG)	0.045	1.08	12.8(9%)	0.70
Tekapo	08 Feb 06	-43.941	170.538	20	57.5(7.5BG)	0.082	0.99	2.9(44%)	0.45
Brunner	10 Feb 06	-42.639	171.445	7	25(5Y)	1.25	4.82	4.3(52%)	0.19
Hochstetter	11 Feb 06	-42.449	171.671	3.5	17.5(7.5YR)	6.24	3.55	5.7(100%)	0.17

\*  $Z_{eu}$ , euphotic depth;  $a_g(440)$ , colored dissolved organic matter (CDOM) absorption at 440 nm ( $m^{-1}$ ); Chl *a*, chlorophyll *a* concentration ( $mg\ m^{-3}$ ); TSS, total suspended solids ( $g\ m^{-3}$ ) (percent organic content given in parentheses);  $b_p(555)$ : TSS, specific particulate scattering coefficient at 555 nm ( $m^2\ g^{-1}$ ) (sample depths were at approximately mid-euphotic depth).

schistose rocks characterized by layer minerals such as micas, with a small proportion in sub-schist greywackes and argillites, which dominate the Tekapo Catchment.

Lakes Brunner and Hochstetter (names commemorating 19th-century pioneer explorer–scientists) are located on the West Coast of South Island on the perhumid western side of the Southern Alps in catchments that receive 2,500–4,000 mm of rainfall annually and that drain extensive wetlands with organic soils or podzolized soils leached of the aluminum and iron oxides that would otherwise immobilize humic substances. These humic-stained lakes have optical properties dominated by CDOM absorption. Both lakes are of fluvio–glacial origin, with catchments mainly in river alluvium from fluvially reworked glacial outwash from the Southern Alps. Lake Hochstetter is notable for its virtually unmodified catchment vegetation, mainly southern beech (*Nothofagus*) forest with kahikatea (*Dacrycarpus dacrydioides*) forest and swamp vegetation near the lake. Table 1 gives station locations and water-quality data pertinent to optical properties.

*In situ profiles*—Field sampling was conducted using jet boats based at National Institute of Water and Atmospheric Research (NIWA) field stations at Tekapo and Greymouth. A side-mounted hydrometric crane, fitted with a calibrated mechanical winch, was used for deploying most of the instrumentation. We sampled a single central (optically deep) station from each lake, commencing with conductivity-temperature-depth (CTD) and light profiles (Seabird 19 Plus CTD, Seabird Electronics, outfitted with a LI-COR LI-193SB scalar quantum sensor) to determine the water column structure and depth of the euphotic zone in order to guide subsequent casts and water collection.

*Inherent optical properties*—We measured in situ profiles of IOPs, the spectral non–water absorption, and beam attenuation coefficients at nine wavelengths (412, 440, 488, 510, 532, 555, 650, and 715 nm) using a WETLabs ac-9 instrument with 0.1-m path length, equipped with a pressure sensor to measure depth. This instrument package was deployed on a custom-built lowering frame that also held a WETLabs ECO-VSF3 instrument for particulate backscattering measurements (*see below*), a Seabird SBE-5T pump to provide water flow to the ac-9, and a WETLabs MPAK unit that controlled pump and instruments and logged data.

Measured absorption and beam attenuation coefficients were corrected for temperature according to the manufacturer’s protocols. We corrected absorption coefficients for scattering errors (Kirk 1992) using a modification of the algorithm of Zaneveld et al. (1994) that subtracts a fraction of measured scattering coefficient from absorption,

$$a_{t-w}(\lambda) = a_m(\lambda) - \varepsilon(c_{t-w}(\lambda) - a_m(\lambda)) \quad (1)$$

where  $a_{t-w}(\lambda)$  is the scattering-corrected absorption coefficient less pure water absorption at wavelength  $\lambda$ ,  $a_m$  is the measured non–water absorption coefficient subject to scattering error,  $c_{t-w}$  is the measured non–water beam attenuation coefficient, and  $\varepsilon$  is a coefficient that accounts

for overall errors with the reflective tube absorption meter of the ac-9, including the following: losses of backscattered light within the reflective tube, losses of a fraction of forward-scattered light owing to the finite acceptance angle of the detector, and imperfect reflection at the wall of the reflective tube. Usually Eq. 1 is employed with the assumption of zero non–water absorption at the longest ac-9 wavelength (715 nm) to calculate  $\varepsilon$ . However, we allowed for some small absorption at 715 nm (Gallegos and Neale 2002; Tassan and Ferrari 2003; Tzortziou et al. 2006), as determined by measurements of absorption in the laboratory. That is,

$$\varepsilon = \frac{a_m(715) - a_{Lab}(715)}{c_{t-w}(715) - a_m(715)} \quad (2)$$

where  $a_{Lab}(715)$  is the absorption measured on a water sample in the laboratory by the quantitative transmittance–reflectance filter pad method (Tassan and Ferrari 1995) and, in the humic lakes, included a small amount of CDOM absorption. Tzortziou et al. (2006) found that this modification was crucial for accurate simulation of water-leaving radiance ( $L_w$ ) and remote-sensing reflectance ( $R_{rs}$ ) in the green region of the spectrum in Chesapeake Bay.

We calculated spectral particulate scattering coefficients,  $b_p(\lambda)$ , from beam attenuation and absorption coefficients according to

$$b_p(\lambda) = c_{t-w}(\lambda) - a_{t-w}(\lambda) \quad (3)$$

and fitted particulate scattering spectra to a power law equation

$$b_p(\lambda) = b_p(555) \left( \frac{555}{\lambda} \right)^\eta \quad (4)$$

where  $\eta$  characterizes the spectral dependence of  $b_p(\lambda)$  and carries information about the size distribution of the particulate matter (Boss et al. 2001).

We used a WETLabs ECO-VSF3 to measure profiles of particulate backscattering at three angles (100°, 125°, and 150°) at each of three visible wavelengths (450, 530, and 650 nm) (Moore et al. 2000). We processed the data according to the manufacturer’s protocols, given by Boss et al. (2004). Briefly, volume scattering coefficients were calculated by applying the factory-determined offset and gain factors to the readings at each wavelength and angle. These coefficients were corrected for loss of photons due to particulate and dissolved absorption along the path length using the temperature- and scattering-corrected  $a_{t-w}(\lambda)$  measured by the ac-9. These corrections were small ( $\leq 1.5\%$ ) in the glacial lakes but were much higher, up to 11% and 80%, at 150° and 450 nm, in (highly absorbing) humic Lakes Brunner and Hochstetter, respectively. Based on prior experience with this particular instrument in the turbid Potomac River (Maryland; C. Gallegos unpubl.), we had the gain factor of the instrument factory-adjusted downward to prevent saturation of the output in the highly reflective glacial lakes. However, this adjustment, together with large absorption correction factors, compromised measurement of particulate backscattering in the humic lakes, as is discussed below.

*Apparent optical properties*—AOPs were measured by two instruments, a TriOS-RAMSES hyperspectral (310–730 nm) radiometer array (TriOS GmbH) and a Satlantic Micropro (Satlantic) seven-waveband (412-, 440-, 488-, 510-, 555-, 670-, and 684-nm) radiometer array. The Satlantic  $E_d$  and  $L_u$  sensors were mounted on a T-frame, which maintained the sensors in a nearly coplanar aspect (25-mm offset). The TriOS sensors incorporate spectrometers built around a 256-channel silicon photodiode array, while the Satlantic sensors are seven-band filter radiometers. Both instrument arrays included reference irradiance sensors ('deck cells'), which were mounted together on a pole fixed to the boat so as to provide an unobstructed view of the incident spectral irradiance,  $E_s$ .

The TriOS radiometer array included an irradiance sensor measuring  $E_d$ , a nadir-viewing radiance sensor ( $7^\circ$  field of view in air) measuring  $L_u$ , as well as the reference irradiance sensor measuring  $E_s$ . The two in-water TriOS instruments were mounted at the end of a 1.2-m-long horizontal boom to minimize interference with the light field by the IOP instrument package at the other end. The diffuser of the sensor measuring downwelling spectral irradiance,  $E_d$ , was used as the reference height (zero of a mechanical winch); this diffuser was mounted 380 mm above the window of the upwelling radiance ( $L_u$ ) sensor. The internal clocks of the TriOS and IOP computers were synchronized and times were recorded at each depth step to permit data sets to be harmonized later. Data collection was initiated at the base of the euphotic zone and continued in depth increments through the water column (2 min at each depth, increments equally spaced except near the surface, where spacing was reduced to improve profile definition).

Data from the TriOS system were logged and processed using the manufacturer's software, which applies offsets and calibration coefficients to all sensors. We multiplied the  $E_d$  and  $L_u$  readings by immersion coefficients calculated according to the method of Ohde and Siegel (2003). We standardized the TriOS radiometers under clear-sky conditions by aiming the  $L_u$  sensor ( $45^\circ$  angle) at a Spectralon Lambertian reflector while measuring incident irradiance with both the zenith-oriented  $E_s$  and  $E_d$  sensors. A normalization-factor spectrum,  $f(\lambda)$ , for correction of  $L_u$  data, was calculated as follows

$$f(\lambda) = \frac{\hat{E}_d(\lambda)}{\pi \hat{L}_u(\lambda)} \quad (5)$$

where  $\hat{L}_u$  and  $\hat{E}_d$  represent the output of the  $L_u$  and  $E_d$  sensors, respectively, in this configuration. The normalization factor, which ranged from 1.02 to 1.07, was multiplied by  $L_u$  readings. For use with RT modeling, we interpolated values from all TriOS sensors in increments of 5 nm from 400 to 700 nm to compensate for the slight wavelength offsets ( $<0.01$  to 1.1 nm) among the sensors.

A separate deployment was made of the Satlantic Micropro sensor array, following standard protocols (Tzortziou et al. 2006). The Satlantic sensors consisted of an OCR-500 upwelling radiance ( $L_u$ ) sensor, an OCI-500 downwelling irradiance ( $E_d$ ) sensor, and an OCI-200

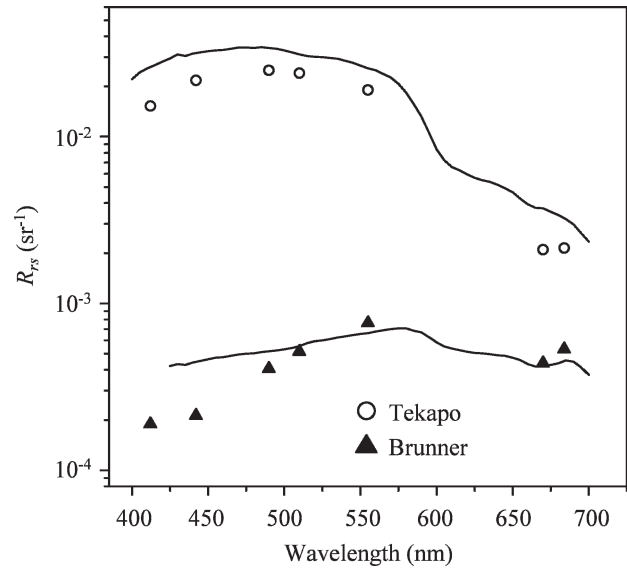


Fig. 2. Comparison of remote sensing reflectance,  $R_{rs}$ , measured using a Satlantic Micropro (symbols) with spectra measured with a TriOS RAMSES hyperspectral radiometer (line) in Lakes Tekapo (open circles) and Brunner (closed triangles).

surface reference ( $E_s$ ) sensor, controlled by a MDU-200 deck unit. Three casts were performed at each station and data were averaged for processing using the manufacturer's software (Level 4). Depths of the profiles were limited by cable length to 10–13 m (and by light penetration to  $\leq 7$  m in Lake Hochstetter). A dark baseline was stored (all three radiometers covered) and the pressure sensor tared at the water surface before profiling began.

Measurements of  $L_u$  by both instrument packages were corrected for instrument self-shading (Gordon and Ding 1992; Zibordi and Ferarri 1995) using non-water absorption coefficients added to pure water absorption coefficients (Pope and Fry 1997). We calculated water-leaving radiance,  $L_w$ , using procedures described in Mueller and Austin (1995). Briefly, we calculated the upwelling radiance immediately beneath the water surface,  $L_u(0^-)$ , by log-linear extrapolation of the three uppermost  $L_u$  readings to the surface, and estimated  $L_w$  as  $0.544 L_u(0^-)$ , where the coefficient accounts for internal reflection and refraction at the air–water interface (Tzortziou et al. 2006). Depths of the uppermost readings ranged from 0.58 to 1.38 m (Lake Hochstetter) to 0.88 to 2.38 m (Lakes Pukaki and Tekapo). Ohde and Siegel (2003) demonstrated good agreement between measurements of  $L_u$  made by TriOS and Satlantic instruments when properly accounting for immersion effects. Our measurements with the two instruments did not agree as well as with theirs, showing twofold differences at blue wavelengths (Fig. 2). Incident irradiance was changeable between profiles, but measurements made of  $R_{rs}$  by the two instruments, incorporating normalizing, agreed fairly well in spectral shape and clearly differentiated the two lakes (Tekapo, Brunner) in which we obtained the full suite of AOPs (Fig. 2). We present results from both instruments using Satlantic measurements for downwelling irradiance and TriOS results for upwelling radiance.

*Laboratory IOPs*—At each station water samples were collected for analysis of LAS and IOPs in the laboratory. A 5-liter GoFlo water sampler (General Oceanics), triggered by a mechanical messenger, was used to collect water from approximately the middle of the euphotic zone. Filtrates for measurement of absorption by CDOM were collected by passing water samples through 47-mm-diameter, 0.2- $\mu\text{m}$  pore-size polycarbonate membrane filters (Nucleopore) into 60-mL glass Schott bottles that had been acid-washed and stored filled with Nanopure water prior to use. The first portion of filtrate was used to rinse the labware and collection bottle before sample collection.

Absorption spectra of CDOM,  $a_g(\lambda)$ , were measured broadly following recommendations outlined in Twardowski et al. (2004). In the laboratory CDOM absorption spectra were measured on filtrates stored in the dark for up to 6 d at 4°C using a dual-beam Shimadzu 2550 ultraviolet (UV) spectrophotometer with cylindrical optical silica cuvettes of 100-mm path length. Samples and blanks (Nanopure water) were measured in the same sample beam using the same cuvette and were referenced to air in the reference beam to minimize beam and cuvette differences. Filtrate samples and Nanopure reference water were maintained at 20°C in a water bath prior to spectral scanning in order to reduce temperature artifacts in absorption spectra. Samples were scanned from 250 to 850 nm at 1-nm intervals with a 1-nm band width.

Absorption spectra of particulate matter,  $a_p(\lambda)$ , were measured by the transmission-reflectance modification of the quantitative filter pad technique (Tassan and Ferrari 1995). A large-volume filtration unit was used for filtrations onto 25-mm GF/F filters. Filters were stored (dark;  $-20^\circ\text{C}$ ) unfolded inside histology cassettes. Absorption spectra were measured in the laboratory using the Shimadzu 2550 UV spectrophotometer (1-nm resolution, 1-nm slit width, 350–850 nm) fitted with an integrating sphere attachment. A customized filter holder (glass slide with black plastic guides) positioned the wetted filter for either reflectance or transmittance measurements. We report only total particulate absorption, because algal pigment extraction using either methanol or sodium hypochlorite also removed appreciable color from the humic lake particulates.

*Attendant water quality measurements*—Color of the lake water, as observed through a black disc viewer (to remove surface reflections), was matched to hue standards in the Munsell system (Davies-Colley et al. 1997). Samples for chlorophyll *a* (Chl *a*) analysis (250 mL) were filtered onto a 25-mm GF/F filter (Whatman). Filters were folded and frozen (ca.  $-20^\circ\text{C}$ ) for subsequent extraction in 90% acetone (4 h) and fluorometric assay (excitation at 435 nm and emission at 675 nm) before and after acidification (Strickland and Parsons 1972).

For total suspended solids (TSS) concentration, a volume of sample was filtered onto preweighed, 47-mm, 0.4- $\mu\text{m}$  polycarbonate (Osmonics brand) filters. For fractional organic content, a larger volume was filtered onto prewashed, precombusted, and preweighed 25-mm GF/F filters, and the weight loss was determined after combustion (400°C for 4 h). Filters were stored in Petri

dishes in the dark prior to laboratory analysis. The polycarbonate filters were desiccated for 2 d and weighed, with a repeat weight the following day to ensure dryness.

*Radiative transfer modeling*—We used the commercially available radiative transfer model, Hydrolight 4.2, which is extensively documented by Mobley (1994). User input consists of specifications for IOPs, boundary conditions, and assumptions on inelastic scattering processes. We used the pure-water absorption coefficients of Pope and Fry (1997) and pure-water scattering coefficients for freshwater from Buiteveld et al. (1994). Except as noted below, we used in situ estimates of absorption, attenuation, and particulate backscattering coefficients binned at 0.5-m intervals. Following the methods of Tzortziou et al. (2006), we used the Fournier–Forand scattering phase function, the shape of which was shown by Mobley et al. (2002) to be well specified by the particulate backscattering ratio. To specify the scattering phase function, we used the ratio of  $b_{bp}(530):b_p(532)$  and attributed this ratio to the wavelength of 530 nm despite the slight wavelength discrepancy between the VSF3 and ac-9 instruments. We included solar-stimulated chlorophyll fluorescence in all runs using depth profiles of chlorophyll concentration estimated from in vivo fluorescence profiles scaled to match the Chl *a* concentration measured at the sampled depth (i.e., half the photic depth; Table 1). We used a specific-absorption spectrum of chlorophyll for Case 2 waters from Gallegos and Neale (2002) and the Hydrolight default fluorescence efficiency and wavelength redistribution function. We used measured incident irradiance (substituting TriOS measurements for Satlantic  $E_s$  at Lake Pukaki where the recorder failed) and assumed calm conditions for the surface boundary condition. For the distribution of total irradiance between direct and sky irradiance we used the built-in RADTRAN routine for the time, location, and estimate of approximate cloud cover. We used the infinitely deep assumption for the bottom boundary, valid at central (optically deep) stations in the study lakes. We omitted Raman scattering after verifying that it contributed negligibly ( $<0.8\%$ ) to simulated  $L_w$  in Lake Tekapo, the clearest of the four lakes. Similarly, we omitted CDOM fluorescence from the Hydrolight simulations, even though it could be appreciable in the humic lakes, because the configuration of our instruments did not permit us to make measurements near enough to the surface to detect it.

Additionally, we tested the accuracy of some commonly used, simple algebraic expressions for diffuse attenuation coefficient,  $K_d$ , given by Kirk (1984, 1994b) and Albert and Mobley (2003). Kirk's (1984) expression takes the form

$$K_d = \frac{1}{\mu_0} [a_t^2 + G(\mu_0)a_t b]^{\frac{1}{2}} \quad (6)$$

where  $\mu_0$  is the cosine of the solar incidence angle after refraction at the air–water interface,  $a_t$  is the total absorption coefficient,  $b$  is the total scattering coefficient, and  $G(\mu_0)$  is a linear function of  $\mu_0$ ,

$$G(\mu_0) = g_1 \mu_0 - g_2 \quad (7)$$

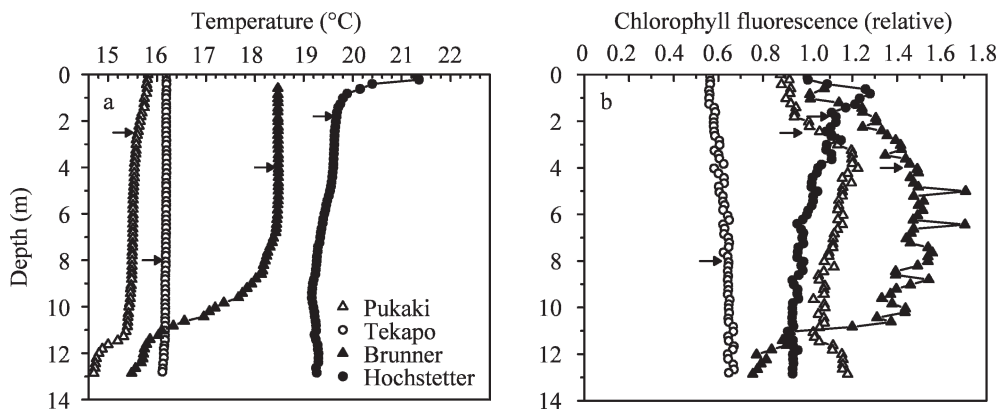


Fig. 3. Vertical profiles of (a) temperature, and (b) chlorophyll fluorescence in (open symbols) glacier-fed and (closed symbols) humic lakes on South Island, New Zealand. Arrows on profiles indicate water sampling depths.

and  $g_1$  and  $g_2$  are coefficients that depend on the shape of the scattering phase function. Kirk (1994b) parameterized  $g_1$  and  $g_2$  in terms of the average cosine of the scattering phase function,  $\bar{\mu}_s$ ,

$$g_1(\bar{\mu}_s) = 2.127\bar{\mu}_s^{-1} - 1.895 \quad (8a)$$

$$g_2(\bar{\mu}_s) = 0.618\bar{\mu}_s^{-1} - 0.490 \quad (8b)$$

We calculated  $\bar{\mu}_s$  from the Fournier–Forand phase function (eqs. 1–2 in Mobley et al. [2002]) and the definition of  $\bar{\mu}_s$  (eq. 3.8b in Mobley [1994]).

Albert and Mobley expressed  $K_d$  as

$$K_d = \kappa_0 \frac{(a_t + b_b)}{\mu_0} \quad (9)$$

where  $b_b$  is the total backscattering coefficient, and  $\kappa_0$  is a coefficient estimated from RT modeling ( $\kappa_0 = 1.0546$  for a particulate backscattering ratio,  $b_{bp} : b_p = 0.019$ ).

**Particle characterization (glacial lakes)**—We measured the particle-size distribution (PSD) of the sample from Lake Pukaki in a Gallai WCIS-100 laser sizer, which estimates size from the time of transit of a focused laser beam across the face of individual particles (in practice, several 1,000s to 10,000s of particles are sized). This was the only one of the four lakes with sufficient particle concentration for direct sizing by this method. We also examined particles from Lakes Pukaki and Tekapo by scanning electron microscopy (SEM). Samples (40 mL) were filtered onto 25-mm polycarbonate 0.2- $\mu\text{m}$  filters (effective filtration area 22 mm in diameter) and stored in the dark at room temperature. The air-dried filters were mounted and sputter-coated with platinum before examination under SEM (Geol JSM-840, 15 KV, 250 mA). Ten random positions were selected for image capture and analysis at magnifications ranging from 1 to  $2 \times 10^4$ .

## Results

**Hydrography and water quality**—Temperatures were lower and profiles were more uniform with depth in the

glacier-fed lakes compared with the humic lakes (Fig. 3a). Certain features of the chlorophyll fluorescence profiles corresponded with the thermal structure (Fig. 3b). Fluorescence was lowest in Lake Tekapo and, like the thermal structure, was nearly uniform, with only a slight increase over the top 13 m (Fig. 3b). Lake Pukaki had a subsurface fluorescence peak below the minor thermocline at 3–4 m and a gradual decline in fluorescence down to the seasonal thermocline, where a jump in fluorescence occurred (Fig. 3b). Lake Brunner had the highest overall fluorescence (Fig. 3b), with a broad subsurface peak from 5 to 8 m and a sharp decline near the thermocline at 11 m. Fluorescence was depressed near the surface in Lake Hochstetter (Fig. 3b), corresponding to the steep near-surface thermocline, below which a Chl *a* fluorescence peak occurred.

Table 1 summarizes the optical water quality of the four lakes. Euphotic depths ranged from 3.5 m in (humic-stained) Lake Hochstetter to 20 m in (glacial) Lake Tekapo, and water sampling depths were approximately at the midpoints of the euphotic zones. Color of the lakes contrasted sharply between the bright gray greenish-blue hue (7.5BG) of the two glacial lakes vs. the very dark-yellow hue (5Y) of Brunner and the orange hue (7.5YR) of Hochstetter (Davies-Colley et al. 2003). CDOM levels were consistent with lake colors, being extremely low (approximately “oceanic” levels; Kirk 1994a, table 3.2) in Tekapo and Pukaki (CDOM absorption coefficients at 440 nm were 0.045 and 0.082  $\text{m}^{-1}$ , respectively), high (1.6  $\text{m}^{-1}$ ) in Brunner, and very high (6.2  $\text{m}^{-1}$ ) in Hochstetter.

Phytoplankton Chl *a* and TSS ranged by only about a fivefold measure among the four lakes (Chl *a*: 0.99–4.8  $\text{mg m}^{-3}$ ; TSS: 2.9–12.8  $\text{g m}^{-3}$ ). Most (55–91%) of the TSS in the glacial lakes was nonvolatile (Table 1), in contrast to the high volatile fraction (52–100%) (phytoplankton, detritus, and aggregated humics) in the humic lakes. SEMs of particulates in Pukaki and Tekapo showed mostly flaky particles (probably mica) with comparatively rare biogenic particles (diatom frustules and rod-shaped bacteria). The PSD for Pukaki particulates had a number median of 0.7  $\mu\text{m}$  (area median = 0.76  $\mu\text{m}$ ), consistent with size estimates from SEMs and the remarkably high

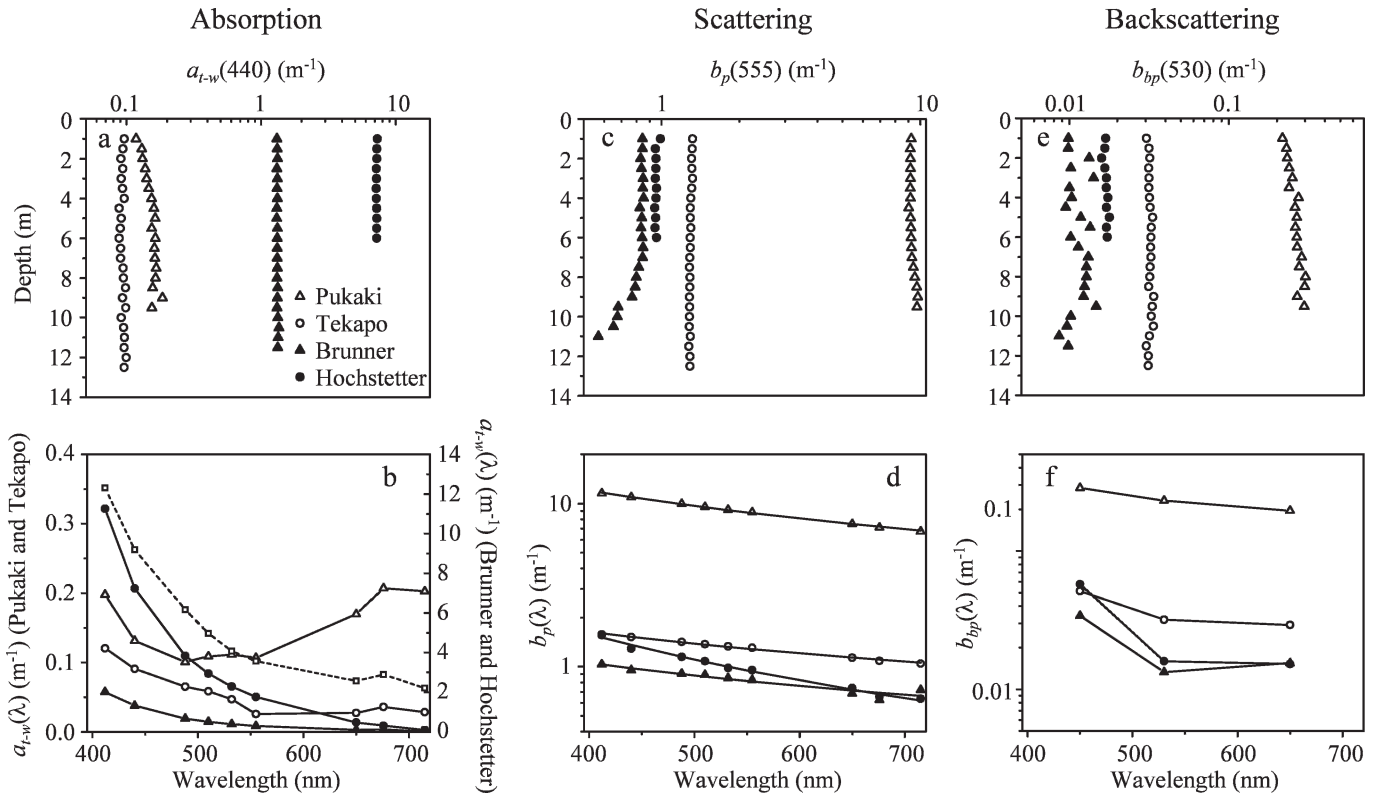


Fig. 4. Vertical profiles and spectra of selected inherent optical properties in four South Island lakes. (a) Vertical profiles of non-water absorption coefficient at 440 nm. (b) Non-water absorption spectra measured using the ac-9 instrument. Note open symbols (for glacier-fed lakes) map to left vertical axis, closed symbols (for the humic lakes) to right axis. Dashed line with open squares represents absorption spectrum for Lake Pukaki corrected for scattering using  $\epsilon$  coefficients determined by measurement of absorption components in the laboratory. (c) Vertical profiles of particulate scattering coefficient at 555 nm. (d) Particulate scattering spectra. Lines are fits of Eq. 4. (e) Vertical profiles of particulate backscattering coefficient at 530 nm. (f) Backscattering coefficients at three wavelengths. All symbols correspond to legend in panel a, and wavelength-dependent panels b, d, and e are from readings at 2 m.

scattering in this lake (below). Mass-specific particulate scattering coefficients [ $b_p(555) : TSS$ ; Table 1] in the glacier-fed lakes were two to three times higher than in the humic lakes, but they were not remarkably high compared with some reports of up to  $2 \text{ m}^2 \text{ g}^{-1}$  from some coastal and oceanic waters (Babin et al. 2003, their fig. 2a).

**IOP profiles**—The four lakes spanned nearly two orders of magnitude in non-water absorption coefficient at 440 nm (Fig. 4a), from ca.  $0.09 \text{ m}^{-1}$  (Lake Tekapo) to ca.  $7 \text{ m}^{-1}$  (Lake Hochstetter). Vertical profiles in  $a_{t-w}(440)$  were nearly uniform. As expected, absorption coefficients were markedly lower in the glacier-fed lakes than in the humic lakes (Fig. 4b, note different scales for glacial lakes—left ordinate, and humic lakes—right ordinate). The U shape of the non-water absorption spectrum in Lake Pukaki was unusual (Fig. 4b), and, as discussed below, we found it necessary to adjust the ac-9 readings for Lake Pukaki using a wavelength-dependent value for  $\epsilon$  (Eq. 1), which resulted in an appreciably shifted absorption spectrum (Fig. 4b) with greater overall range (0.1–0.38  $\text{m}^{-1}$ ) and a spectral shape similar to that measured in Lake Tekapo. Absorption spectra in the humic lakes (Fig. 4b) exhibited the expected negative exponential shape characteristic of CDOM absorption.

Particulate scattering coefficients at 555 nm varied by an order of magnitude among the four lakes, from  $0.8 \text{ m}^{-1}$  in Lake Brunner to  $9 \text{ m}^{-1}$  in Lake Pukaki (Fig. 4c). Profiles in the lakes were relatively uniform with depth, except in Lake Brunner, where  $b_p(555)$  declined near the thermocline base (Fig. 3a). This was the only feature in the vertical profiles of IOPs that was clearly associated with a hydrographic feature, paralleling the decline in the fluorescence depth profile (cf. Fig. 3b).

All particulate scattering spectra were declining functions of wavelength (Fig. 4d) and were well fit by a power law (Eq. 4) (Fig. 4d; minimum  $r^2 = 0.926$ , maximum absolute residual 10%). Lake Hochstetter had by far the highest particulate scattering spectral exponent ( $\eta = 1.61$ ), with appreciably lower values in Lakes Pukaki (0.97), Brunner (0.80), and Tekapo (0.75). Particulate backscattering coefficients at 530 nm varied by a 20-fold measure among the four lakes (Fig. 4e), from ca.  $0.015 \text{ m}^{-1}$  in Lake Brunner to  $0.2\text{--}0.3 \text{ m}^{-1}$  in Lake Pukaki. Vertical profiles of  $b_{bp}(530)$  were nearly uniform with depth, except for a gradual increasing trend in Lake Pukaki (Fig. 4e). The particulate backscattering profile at Lake Brunner suffered considerable noise, because the raw readings were only four to seven counts (out of 4,095 full scale) above the pure water offsets. The shapes of particulate backscattering

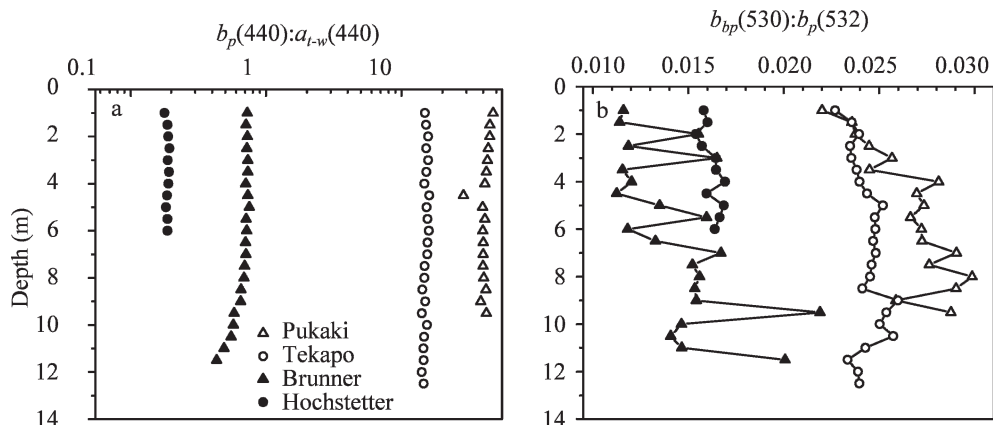


Fig. 5. Vertical profiles of (a) particulate scattering:non-water absorption ratio at 440 nm and (b) ratio of particulate backscattering:total particulate scattering (backscatter fraction) at 530 nm.

spectra were not well resolved by only three wavelengths (Fig. 4f), but coefficients declined with increasing wavelengths in Lakes Pukaki and Tekapo, but only from the blue to green wavelengths in the humic lakes. The combination of low counts and low instrument gain (adjusted to keep measurements on scale in Lake Pukaki) resulted in barely detectable particulate backscattering in Lakes Brunner and Hochstetter.

The particulate scattering:non-water absorption ratios at 440 nm varied by a 200-fold measure among the four lakes, from 0.2 in Hochstetter to 45 in Pukaki (Fig. 5a). The ratios were very high ( $>10$ ) in both glacier-fed lakes and very low ( $<1$ ) in the two humic lakes—consistent with the water color. The particulate backscattering fraction at (nominally) 530 nm was similar near the surface in the two glacier-fed lakes (ca. 0.022; Fig. 5b) and higher than in the humic lakes. These estimates for the humic lakes may be too high still as a result of the aforementioned discretization errors in particulate backscatter coefficients, as indicated by the data noise, particularly for Lake Brunner (Fig. 5b). For radiative transfer modeling of these lakes, we assumed a constant particulate backscattering fraction measured as the depth-averaged value at green wavelengths, 0.0115 for Lake Brunner and 0.016 for Lake Hochstetter.

*AOPs and closure modeling*—The depth profile of downwelling spectral irradiance increased in slope (i.e., rate of attenuation) from glacier-fed to humic lakes in the same order as absorption (i.e., Tekapo  $<$  Pukaki  $<$  Brunner  $<$  Hochstetter; Fig. 6a, profile shown at 442 nm, a wavelength at which all LAS contribute to absorption). Hydrolight estimates of  $E_d(442)$  consistently exceeded measurements in Lake Pukaki (Fig. 6a), and the deviation of modeled from measured  $E_d$  increased with depth, a result that is symptomatic of the distorted absorption spectrum measured in that lake (see corrected spectrum, Fig. 4b). Simulations of  $E_d(442)$  for the other lakes did not accumulate systematic errors with depth, as in the case of Lake Pukaki (Fig. 6a). Specific adjustments to IOPs that improved model fits (Figs. 6a,b, 7a,b) are discussed in detail below (see Discussion).

Overall, spectral diffuse attenuation coefficients ranged 50-fold from a minimum of  $0.196 \text{ m}^{-1}$  at 490 nm in Lake Tekapo to  $12.2 \text{ m}^{-1}$  at 412 nm in Lake Hochstetter (Fig. 6b). Both magnitude and shape of diffuse attenuation spectra were well predicted by Hydrolight for Lakes Tekapo, Brunner, and Hochstetter. In Lake Pukaki there was a systematic tendency to underpredict  $K_d(\lambda)$  at short visible wavelengths and to overpredict at longer wavelengths (Fig. 6b), casting doubt on the unusually shaped absorption spectrum measured in that lake (Fig. 4b). Over the complete range of measurements, the root-mean-square error (RMSE) of Hydrolight predictions of  $K_d$  was  $0.304 \text{ m}^{-1}$ , with a relative RMSE (RRMSE, the RMS of percent deviations) of 13.4% (Fig. 6c; Table 2).

Equation 6 fit measured  $K_d$  slightly better than the Hydrolight simulations (RRMSE = 6.1%), while the expression of Albert and Mobley (2003) fit slightly worse (RRMSE = 18.8%), mostly as the result of an approximately 33% underestimate of  $K_d$  in Lake Pukaki (Fig. 6d). For Lake Pukaki, calculation of the coefficients  $g_1$  and  $g_2$  according to Eqs. 8a and 8b made a slight improvement in calculated  $K_d(\lambda)$  (compared with Kirk's [1984] original estimates,  $g_1 = 0.425$  and  $g_2 = 0.19$ ) and an insignificant difference in the other lakes.

Hydrolight provided slightly lower values of  $L_u(440)$  compared with measurements at Lake Tekapo, but predictions of the vertical profile paralleled measurements (Fig. 7a). However,  $L_u(440)$  was overpredicted at all depths in Lake Pukaki (Fig. 7a), and predictions diverged increasingly from measurements with increasing depth, as was the case with  $E_d(442)$  (Fig. 6a). The model-predicted profiles of  $L_u$  were close to and parallel with measurements in Lakes Brunner and Hochstetter (Fig. 7a). Note that measured and modeled  $L_u$  are reported at 530 nm (rather than 440 nm) for Lake Hochstetter because of the very low radiance below 490 nm in this lake. Similarly,  $L_u$  measurements became erratic at wavelengths of  $<420 \text{ nm}$  in Lake Brunner.

The quality of the Hydrolight fits to the water-leaving radiance spectra,  $L_w(\lambda)$ , varied among the lakes. At Lake Pukaki there was a tendency to overpredict  $L_w$  slightly at wavelengths of  $<500 \text{ nm}$  and to underpredict  $L_w$  at

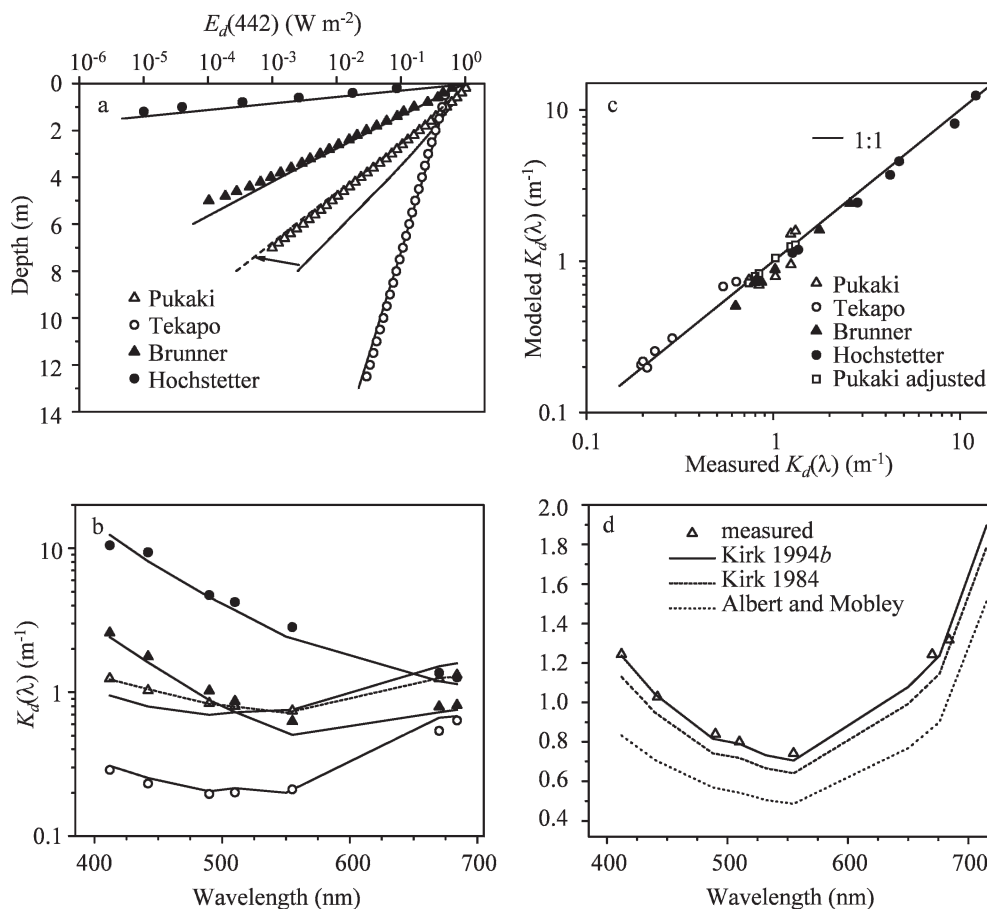


Fig. 6. (a) Vertical profiles of measured (symbols) and Hydrolight modeled (lines) downwelling spectral irradiance at 442 nm. (b) Spectra of measured (symbols) and Hydrolight modeled (lines) diffuse attenuation coefficients. (c) Comparison of Hydrolight modeled with measured spectral diffuse attenuation coefficients. Line of 1 : 1 agreement is shown for reference. (Corresponding statistics are given in Table 2.) (d) Comparison of measured diffuse attenuation spectrum (symbols) with those calculated by simple analytical expressions: dotted line, Eq. 9; dashed line, Eqs. 6, 7,  $g_1 = 0.425$ ,  $g_2 = 0.19$  (Kirk 1984); solid line, Eqs. 6–8 (Kirk 1994b). Dashed lines for Lake Pukaki in panels a and b, all lines in panel d, and open squares in panel c are calculations after adjustment for wavelength dependence of ac-9 scattering correction factors for Lake Pukaki based on laboratory absorption measurements (*see text*).

wavelengths of  $>570$  nm (Fig. 7b), an inverse trend to that of  $K_d(\lambda)$  (cf. Fig. 6b). The model tended to underpredict  $L_w$  at all wavelengths in Lake Tekapo (Fig. 7b), but predictions captured the spectral shape of the measurements. Model predictions for Lakes Brunner and Hochstetter conformed well with measurements, except at blue wavelengths, in which the  $L_u$  signal became very small (Fig. 7b).

Because of the contrasting optical properties of the four lakes, points on the plot of model-predicted vs. measured  $L_w$  fell into four clusters (Fig. 7c). For context, we include the Chesapeake Bay data of Tzortziou et al. (2006, derived from their fig. 9), which mostly fell between the clusters belonging to Lakes Pukaki and Brunner (Fig. 7c). Our measured  $L_w$  values extend the main cluster of their measurements by about an order of magnitude in each direction. Agreement between lake  $L_w$  predictions and measurements ranged between 12% and 23% (RRMSE; Table 2) and measured 17% when considering all lakes

together. The largest deviations were for Lake Pukaki (Table 2); we attribute these deviations to the systematic overprediction of measurements at wavelengths less than 500 nm and to underprediction at wavelengths greater than ca. 580 nm (cf. Fig. 7b). Given the accuracy of Hydrolight estimates in the other lakes, we suspect that difficulties lie with measured IOPs in Lake Pukaki rather than with the radiative transfer model, as we discuss below.

### Discussion

*Optical properties of extreme lakes*—The four lakes studied here provided an extreme contrast in optical properties by virtue of their differing types and amounts of LAS. The lakes ranged by only about a fivefold measure in terms of TSS and phytoplankton biomass, but they ranged by more than two orders of magnitude in CDOM, from levels characteristic of oligotrophic oceanic water to

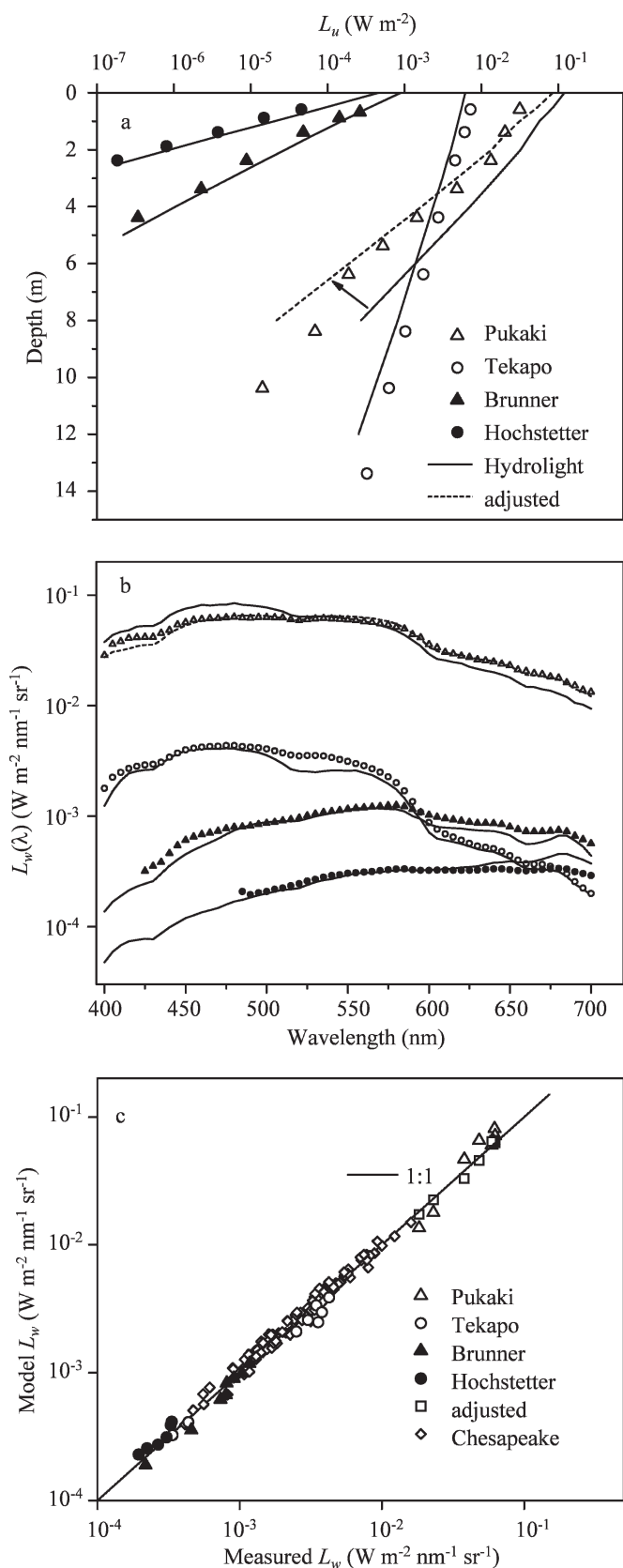


Fig. 7. (a) Vertical profiles of measured (symbols) and Hydrolight modeled (lines) upwelling radiance ( $L_u$ ) at 440 nm (530 nm in Lake Hochstetter [closed circles], where there was

very high levels characteristic of wetland drainage (Kirk 1994a: his table 3.2). This marked contrast in optical water quality challenged optical closure at the extremes of reflectance of natural waters.

Non-water absorption and scattering coefficients varied among the lakes in magnitude and spectral shapes in ways that were expected given the relative amounts and dominant types of LAS (Fig. 4). The  $b_p:a_{t-w}$  ratio for Lake Pukaki was near the maximum expected for natural waters (ca. 45; Loisel and Morel 2001). Particulate backscattering properties of the lakes, however, were not as extreme as might have been expected. Particulate backscatter fractions in the lakes dominated by mineral suspensoids varied from 0.022 to 0.03 (Fig. 5b); mostly these values were somewhat lower than the value (0.03) used by Stramski et al. (2001) to characterize backscattering by oceanic minerals and were near the middle of the range (0.0024–0.0417) observed by Loisel et al. (2007). The difference, though not large, is consistent with the fact that the lakes are not pure suspensions of glacial flour. The bulk particulate backscatter fraction is necessarily smaller than that of the component having the highest value in isolation (Peng et al. 2007). Similarly, particulate backscattering fractions for the humic lakes (ca. 0.012–0.016; Fig. 5b) were larger than expected for waters dominated by organic detritus. Stramski et al. (2004) used 0.005 as a characteristic backscattering fraction for detritus, but for Case 1 waters, in which this component derives from phytoplankton.

The particulate scattering spectral exponents for the humic lakes (Eq. 4;  $\eta = 0.80$  and 1.61 for Lakes Brunner and Hochstetter, respectively) were relatively high, which is broadly indicative of scattering by small particles (Boss et al. 2001) and which could contribute to higher-than-expected particulate backscattering fraction. Gallegos (2005) found that  $\eta$  was positively correlated with CDOM absorption [ $r = 0.74$ , with  $a_g(440)$  up to  $28 m^{-1}$ ] in the tidal fresh portion of the very strongly humic-stained St. Johns River (Florida), indicating that very fine, possibly colloidal, particulate matter (presumably aggregated humics) may accompany very high CDOM concentrations and contribute to backscattering in humic-dominated systems, as has been suggested also for the ocean (Stramski et al. 2004).

The extreme range of IOPs observed in the four lakes provided a good test of some commonly used simple formulae derived from RT modeling (Eqs. 6, 9). Accurate specification of  $a_t$  and  $b$  are of primary importance for

←

insufficient signal at wavelengths of  $<480$  nm). The arrow connects the model profile before (solid line) and after (dashed line) adjustment of IOPs for Lake Pukaki (see text). (b) Spectra of measured (symbols) and Hydrolight modeled (lines) water-leaving radiance. (c) Comparison of Hydrolight modeled with measured water-leaving radiance at visible wavelengths corresponding to ac-9 measurements. Line of 1:1 agreement is shown for reference. (Corresponding statistics are given in Table 2.) Open squares in panel c are Hydrolight output after adjustment of absorption spectrum for Lake Pukaki (see text). Open diamonds in panel c are data of Tzortziou et al. (2006) from Chesapeake Bay, shown to provide context for measurements reported here.

Table 2. Statistics of Hydrolight model fits to observed spectral diffuse attenuation coefficients,  $K_d(\lambda)$ , and water-leaving radiance,  $L_w(\lambda)$ , in four lakes. Data are given before and after adjustment of inherent optical properties (IOPs) for Lake Pukaki as described in the text (compare Figs. 6c, 7c).

Lake	$K_d$				$L_w$			
	In situ IOPs		Adjusted IOPs		In situ IOPs		Adjusted IOPs	
	RMSE	RRMSE	RMSE	RRMSE	RMSE	RRMSE	RMSE	RRMSE
Pukaki	0.212	18.4	0.02	1.9	0.01043	22.7	0.00335	7.4
Tekapo	0.052	10.8			0.00051	15.3		
Brunner	0.127	12.3			0.00007	12.2		
Hochstetter	0.552	10.7			0.00005	15.6		
All lakes combined	0.304	13.4	0.29	9.8	0.00539	17.0	0.00175	12.8

RMSE, root-mean-square error, with units of associated parameter:  $K_d$  ( $m^{-1}$ );  $L_w$  ( $W m^{-2} nm^{-1} sr^{-1}$ ); RRMSE (relative root-mean-square error) RMS of percent deviations.

predicting  $K_d$  in all waters (McKee et al. 2003b), but in Lake Pukaki, it was also necessary to account for the shape of the scattering phase function (Fig. 6d). The success of Kirk’s (1994b) parameterization of  $g_1$  and  $g_2$  (Eq. 8) indicates that a similar parameterization in terms of  $\bar{\mu}_s$  or

$b_b : b$  would be worthwhile for coefficients in other simple relationships. Considerable guidance for the range of  $b_{bp} : b_p$  (from which total  $b_b : b$  is easily calculated) is now available in the literature (Boss et al. 2004; Loisel et al. 2007; Snyder et al. 2008), which indicates that  $b_{bp} : b_p$  is highly variable and that the average in coastal waters is lower than the value of 0.019 commonly assumed in RT simulations used to derive simple formulae.

*Diagnosis of errors*—The extremely high scattering and absorption characterizing the contrasting lakes we studied pose severe challenges for the instruments measuring IOPs and AOPs, and these challenges translate into difficulties obtaining optical closure. Relationships between AOPs and IOPs derived from radiative transfer theory can help identify the measurement likely to be in error when closure is not achieved. For diffuse attenuation, Eqs. 6 and 9 indicate direct dependence of  $K_d$  on absorption. The relationship between remote sensing reflectance, ( $R_{rs}$ ), and IOPs (Gordon and Morel 1983),

$$R_{rs} \equiv \frac{L_w}{E_s} \propto \frac{b_b}{a + b_b} \quad (10)$$

implies an inverse relationship between  $L_w$  and  $a$ . For Lake Pukaki, the tendency for Hydrolight to underpredict  $K_d$  at short visible wavelengths (<555 nm) and to overpredict at longer wavelengths, together with the inverse trend in  $L_w$  (cf. Figs. 6b, 7b), indicates a systematic spectral bias in measured absorption, on consideration of Eqs. 9 and 10. The increasing spectral absorption from 555 to 715 nm (Fig. 4b) precluded the use of the standard ac-9 scattering correction (Zaneveld et al. 1994), even allowing for some particulate absorption at 715 nm (Gallegos and Neale 2002; Tzortziou et al. 2006). This upward trend in  $a_{t-w}(\lambda)$  from 555 to 715 nm was observed both in field spectra (Fig. 4b) and in a lake-water sample scanned in the ac-9 (in the laboratory) immediately after cleaning. We calculated wavelength-dependent correction factors,  $\varepsilon(\lambda)$ , using absorption spectra measured in the laboratory, substituting  $a_{Lab}(\lambda) [=a_p(\lambda) + a_g(\lambda)]$  for  $a_{Lab}(715)$  in Eq. 2, i.e.,

$$\varepsilon(\lambda) = \frac{a_m(\lambda) - a_{Lab}(\lambda)}{c_{t-w}(\lambda) - a_m(\lambda)} \quad (11)$$

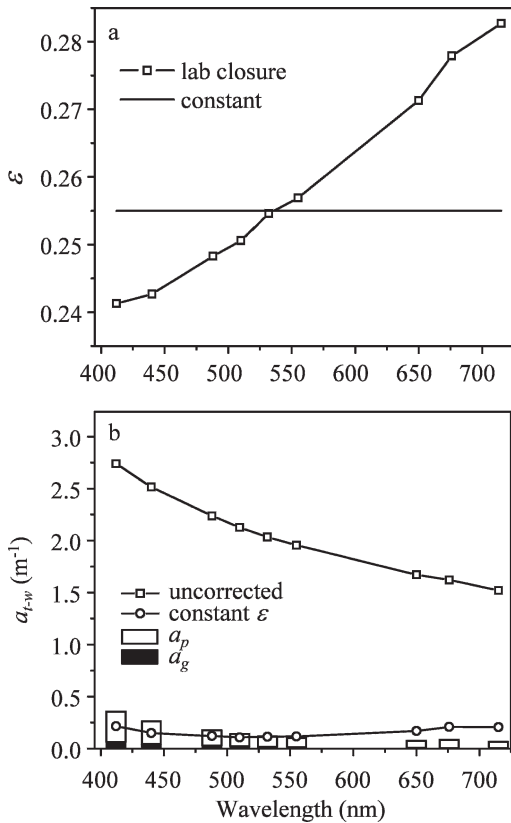


Fig. 8. (a) Spectral variation of ac-9 scattering correction factor,  $\varepsilon$ , determined by forcing agreement between ac-9 readings and laboratory partitioning of particulate plus dissolved absorption (bars in panel b) in a water sample from Lake Pukaki. Horizontal solid line at  $\varepsilon = 0.255$  is value used for Hydrolight simulation prior to adjustment. (b) Non-water absorption coefficients for water sample from Lake Pukaki measured by the ac-9 without correction (squares) and corrected using constant  $\varepsilon$  (circles). Laboratory measurements of particulate ( $a_p$ , open bars) plus dissolved ( $a_g$ , solid bars) absorption [which sum to  $a_{Lab}(\lambda)$ , Eq. 11] were used to calculate wavelength-dependent  $\varepsilon$  coefficients in panel a.

$\varepsilon(\lambda)$  increased monotonically with wavelength (Fig. 8a). These coefficients depend on fixed properties of the ac-9 instrument (tube diameter, reflectivity, acceptance angle of the detector) and the scattering phase function of the sample (Kirk 1992). Use of the adjusted correction factors yielded non-water absorption coefficients larger than the constant- $\varepsilon$  estimates by nearly a factor of two at blue wavelengths and smaller by a factor of two to three at red wavelengths (Fig. 8b). When we used absorption coefficients calculated with these wavelength-dependent  $\varepsilon$  values in Hydrolight, the systematic spectral bias in  $K_d$  and  $L_w$  for Lake Pukaki was largely removed (Figs. 6b, 7b). Note that this adjustment procedure is *not* equivalent to driving the simulation with laboratory absorption measurements (measured on a sample from only one depth), because the optical stratification, though not large during measurements in these lakes, is retained in the simulation.

The overall comparison of model with measured  $K_d$  improved with adjustment of  $\varepsilon(\lambda)$ , from about 13% to 10%, while agreement for  $L_w$  improved from 17% to about 13% (Figs. 6c, 7c; Table 2). The overall agreement for  $L_w$ , obtained after adjustment of  $\varepsilon$ , was comparable to that obtained by Tzortziou et al. (2006) in the optically complex, although less extreme, waters of Chesapeake Bay.

*Enduring challenges for measuring IOPs*—Problems of absorption measurement with the ac-9 due to wavelength dependence of the scattering correction factor have been described previously for waters with abundant, highly scattering coccoliths (Smyth et al. 2002; McKee et al. 2003a). To compensate for uncertainties in ac-9 performance, Smyth et al. (2002) used absorption coefficients generated by a bio-optical model, while McKee et al. (2003a) used Hydrolight to infer the magnitude of wavelength dependence of the ac-9 correction factor. Our adjustments to the correction factors for Lake Pukaki were based on measured (principally particulate) absorption coefficients and therefore were independent of the Hydrolight output. Our assumption of spectrally constant  $b_{bp}:b_p$  in Lakes Brunner and Hochstetter was necessitated by noisy readings owing to the downward adjustment of the gain on the ECO-VSF3 (to prevent saturation of the instrument in glacier-fed lakes studied in the same field campaign). While these adjustments seem reasonable and defensible, any need to make such adjustments falls short of the closure ideal of predicting AOPs from IOPs measured in situ. Nevertheless, our measurements in Lake Tekapo met this objective, and the adjustments to absorption measurements in Lake Pukaki were needed only to achieve relatively fine-scale spectral tuning of modeled  $L_w$  (Fig. 7b; Table 2). Even without these adjustments we were able to obtain agreement with observations to within 17%, including measurements of  $L_w$  that measured up to fivefold higher than previously published closure studies (Bulgarelli et al. 2003; Chang et al. 2003; Tzortziou et al. 2006).

The problems with the absorption measurements in Lake Pukaki (by comparison with broadly comparable Lake Tekapo) are worthy of further note. We do not believe that the amount of scattering per se was the source of the difficulty. Beam attenuation coefficients in Lake Pukaki

were no higher than some profiles measured by Tzortziou et al. (2006), which caused no particular problems for closure modeling, despite multiple scattering. The difficulties we encountered in Lake Pukaki seem to reflect a very high  $b_p:a_{t-w}$  ratio, whereby very low non-water absorption is being measured in the presence of very high particulate scattering, so that the uncorrected absorption coefficients were dominated by the scattering error (Fig. 8b). Key to the difficulties in Lake Pukaki was the increase in non-water absorption coefficient from 555 to 715 nm, which precluded using the standard scattering correction procedure. However, this spectral trend was not measured by laboratory partitioning of dissolved and particulate absorption components (Fig. 8b), and there was only a slight indication of it in (broadly comparable, glacier-fed) Lake Tekapo (Fig. 3b). We believe the phenomenon may reflect interaction between multiple scattering and molecular water absorption when scattering is high and absorption by other LAS is low. Future work in waters with high  $b_p:a_{t-w}$  would benefit from measurements with absorption meters that do not require scattering correction (e.g., integrating cavity; Röttgers et al. 2005).

The qualified success of our optical closure modeling of both humic- and glacial flour-dominated waters of highly contrasting reflectance indicates that AOPs of coastal waters receiving discharges of mineral suspensoids and humic matter could be confidently predicted by transport models for the limiting case in which the LAS behave conservatively on mixing. The limiting case, however, is not the likely case, as colloids tend to flocculate upon mixing with water of high ionic strength, and CDOM may adsorb to particulates or flocculate (Uher et al. 2001) and is subject to photobleaching and microbial processing. Such transformations can alter amounts and optical properties of the LAS. Our observations provide a benchmark for assessing the magnitude of such transformations—by comparing in situ measured AOPs with predictions assuming conservation of light attenuation. As the prediction of the bulk IOPs of a water body from the composition of the particulate matter progresses (Gordon and Du 2001; Stramski et al. 2001), environments such as estuaries and coastal river plumes, in which IOPs change rapidly, represent fresh challenges for theoretical and observational studies.

## References

- ALBERT, A., AND C. D. MOBLEY. 2003. An analytical model for subsurface irradiance and remote sensing reflectance in deep and shallow case-2 waters. *Optics Express* **11**: 2873–2890.
- BABIN, M., A. MOREL, V. FOURNIER-SICRE, F. FELL, AND D. STRAMSKI. 2003. Light scattering properties of marine particles in coastal and open ocean waters as related to the particle mass concentration. *Limnol. Oceanogr.* **48**: 843–859.
- , AND D. STRAMSKI. 2004. Variations in the mass-specific absorption coefficient of mineral particles suspended in water. *Limnol. Oceanogr.* **49**: 756–767.
- BOSS, E., W. S. PEGAU, M. LEE, M. S. TWARDOWSKI, E. SHYBANOV, AND G. KOROTAEV. 2004. Particulate backscattering ratio at LEO 15 and its use to study particle composition and distribution. *J. Geophys. Res.* **109**: C01014, doi:10.1029/2002JC001514.

- , M. S. TWARDOWSKI, AND S. HERRING. 2001. Shape of the particulate beam attenuation spectrum and its inversion to obtain the shape of the particulate size distribution. *Appl. Optics* **41**: 4885–4893.
- BUI TEVELD, H., J. H. M. HAKVOORT, AND M. DONZE. 1994. The optical properties of pure water, p. 174–183. *In* J. F. Jaffe [ed.], *Ocean optics XII*. Society of PhotoOptical Engineering.
- BULGARELLI, B., Z. GIUSEPPE, AND J.-F. BERTHON. 2003. Measured and modeled radiometric quantities in coastal waters: Toward a closure. *Appl. Optics* **42**: 5365–5381.
- CHANG, G., T. D. DICKEY, C. D. MOBLEY, E. BOSS, AND W. S. PEGAU. 2003. Toward closure of upwelling radiance in coastal waters. *Appl. Optics* **42**: 1574–1582.
- DAVIES-COLLEY, R. J., D. G. SMITH, D. J. SPEED, AND J. W. NAGELS. 1997. Matching natural water colors to Munsell standards. *J. Am. Water Resour. Assoc.* **33**: 1351–1361.
- , W. N. VANT, AND D. G. SMITH. 2003. Colour and clarity of natural waters: Science and management of optical water quality. The Blackburn Press.
- GALLEGOS, C. L. 2005. Optical water quality of a blackwater river estuary: The Lower St. Johns River, Florida, USA. *Estuar. Coast. Shelf Sci.* **63**: 57–72.
- , AND P. J. NEALE. 2002. Partitioning spectral absorption in case 2 waters: Discrimination of dissolved and particulate components. *Appl. Optics* **41**: 4220–4233.
- GORDON, H. R., AND K. DING. 1992. Self-shading of in-water optical instruments. *Limnol. Oceanogr.* **37**: 491–500.
- , AND T. DU. 2001. Light scattering by nonspherical particles: Applications to coccoliths detached from *Emiliana huxleyi*. *Limnol. Oceanogr.* **46**: 1438–1454.
- , AND A. Y. MOREL. 1983. Remote assessment of ocean color for interpretation of satellite visible imagery. A review. Springer-Verlag.
- KIRK, J. T. O. 1984. Dependence of relationship between apparent and inherent optical properties of water on solar altitude. *Limnol. Oceanogr.* **29**: 350–356.
- . 1992. Monte Carlo modeling of the performance of a reflective tube absorption meter. *Appl. Optics* **31**: 6463–6468.
- . 1994a. Light and photosynthesis in aquatic ecosystems. Cambridge Univ. Press.
- . 1994b. The relationship between the inherent and the apparent optical properties of surface waters and its dependence on the shape of the volume scattering function, p. 40–58. *In* R. W. Spinrad, K. L. Carder and M. J. Perry [eds.], *Ocean optics*. Oxford Monographs on Geology and Geophysics. Oxford Univ. Press.
- LOISEL, H., X. MÉRIAUX, J.-F. BERTHON, AND A. POTEAU. 2007. Investigation of the optical backscattering to scattering ratio of marine particles in relation to their biogeochemical composition in the eastern English Channel and southern North Sea. *Limnol. Oceanogr.* **52**: 739–752.
- , AND A. MOREL. 2001. Non-isotropy of the upward radiance field in typical coastal (case 2) waters. *Int. J. Remote Sens.* **22**: 275–295.
- MAGNUSON, A., L. W. HARDING, JR., M. E. MALLONEE, AND J. E. ADOLF. 2004. Bio-optical model for Chesapeake Bay and the Middle Atlantic Bight. *Estuar. Coast. Shelf Sci.* **61**: 403–424.
- McKEE, D., A. CUNNINGHAM, AND S. CRAIG. 2003a. Semi-empirical correction algorithm for AC-9 measurements in a coccolithophore bloom. *Appl. Optics* **42**: 4369–4374.
- , ———, J. SLATER, K. J. JONES, AND C. R. GRIFFITHS. 2003b. Inherent and apparent optical properties in coastal waters: A study of the Clyde Sea in early summer. *Estuar. Coast. Shelf Sci.* **56**: 369–376.
- MOBLEY, C. D. 1994. Light and water. Radiative transfer in natural waters. Academic Press.
- , L. K. SUNDMAN, AND E. BOSS. 2002. Phase function effects on oceanic light fields. *Appl. Optics* **41**: 1035–1050.
- MOORE, C., M. S. TWARDOWSKI, AND J. R. V. ZANEVELD. 2000. The ECO VSF—a multi-angle scattering sensor for determination of the volume scattering function in the backward direction. *In* S. G. Ackleson and J. Marra [eds.], *Proceedings from Ocean Optics XV*, October 16–20. Monaco: SPIE.
- MOREL, A. 1988. Optical modeling of the upper ocean in relation to its biogenous matter content (case I waters). *J. Geophys. Res.* **93**: 10749–10768.
- MUELLER, J. L., AND R. W. AUSTIN. 1995. Ocean optics protocols for SeaWiFS validation, revision 1, p. 1–65. *In* S. B. Hooker, E. R. Firestone and J. G. Acker [eds.], *SeaWiFS technical report series*. National Aeronautics and Space Association.
- OHDE, T., AND H. SIEGEL. 2003. Derivation of immersion factors for the hyperspectral TriOS radiance sensor. *J. Optics A Pure Appl. Optics* **5**: 13–15.
- PENG, F., S. W. EFFLER, D. O'DONNELL, M. G. PERKINS, AND A. WEIDEMANN. 2007. Role of minerogenic particles in light scattering in lakes and a river in central New York. *Appl. Optics* **46**: 6577–6594.
- POPE, R. M., AND E. S. FRY. 1997. Absorption spectrum (380–700) nm of pure water. II. Integrating cavity measurements. *Appl. Optics* **36**: 8710–8723.
- RÖTTGERS, R., W. SCHÖNFELD, P.-R. KIPP, AND R. DOERFFER. 2005. Practical test of a point-source integrating cavity absorption meter: The performance of different collector assemblies. *Appl. Optics* **44**: 5549–5560.
- SMYTH, T. J., G. F. MOORE, S. B. GROOM, P. E. LAND, AND T. TYRRELL. 2002. Optical modeling and measurements of a coccolithophore bloom. *Appl. Optics* **41**: 7679–7688.
- SNYDER, W. A., AND OTHERS. 2008. Optical scattering and backscattering by organic and inorganic particulates in U.S. coastal waters. *Appl. Optics* **47**: 666–677.
- STRAMSKI, D., E. BOSS, D. BOGUCKI, AND K. J. VOSS. 2004. The role of seawater constituents in light backscattering in the ocean. *Prog. Oceanogr.* **61**: 27–56.
- , A. BRICAUD, AND A. MOREL. 2001. Modeling the inherent optical properties of the ocean based on the detailed composition of the planktonic community. *Appl. Optics* **40**: 2929–2945.
- STRICKLAND, J. D. H., AND T. R. PARSONS. 1972. A practical handbook of seawater analysis, 2nd ed. Fisheries Research Board of Canada.
- TASSAN, S., AND G. M. FERRARI. 2003. Variability of light absorption by aquatic particles in the near-infrared spectral region. *Appl. Optics* **42**: 4802–4810.
- , AND M. FERRARI. 1995. An alternative approach to absorption measurements of aquatic particles retained on filters. *Limnol. Oceanogr.* **40**: 1358–1368.
- TWARDOWSKI, M. S., E. BOSS, J. S. SULLIVAN, AND P. L. DONAGHAY. 2004. Modeling the spectral shape of absorption by chromophoric dissolved organic matter. *Mar. Chem.* **89**: 69–88.
- TZORTZIOU, M., J. R. HERMAN, C. L. GALLEGOS, P. J. NEALE, A. SUBRAMANIAM, AND L. W. HARDING, JR. 2006. Bio-optics of the Chesapeake Bay from measurements and radiative transfer closure. *Estuar. Coast. Shelf Sci.* **68**: 348–362.
- , A. SUBRAMANIAM, J. R. HERMAN, C. L. GALLEGOS, P. J. NEALE, AND L. W. HARDING, JR. 2007. Remote sensing reflectance and inherent optical properties in the mid Chesapeake Bay. *Estuar. Coast. Shelf Sci.* **72**: 16–32.
- UHER, G., C. HUGHES, G. HENRY, AND R. C. UPSTILL-GODDARD. 2001. Non-conservative mixing behavior of colored dissolved organic matter in a humic-rich, turbid estuary. *Geophys. Res. Lett.* **28**: 3309–3312.

- VANT, W. N., AND R. J. DAVIES-COLLEY. 1984. Factors affecting clarity of New Zealand lakes. *N. Z. J. Mar. Freshw. Res.* **18**: 367–377.
- ZANEVELD, J. R. V. 1994. Optical closure: From theory to measurement, p. 59–72. *In* R. W. Spinrad, K. L. Carder and M. J. Perry [eds.], *Ocean optics*. Oxford Monographs on Geology and Geophysics. Oxford Univ. Press.
- , J. C. KITCHEN, AND C. MOORE. 1994. The scattering error correction of reflecting-tube absorption meters, p. 44–55. *In* S. Ackleson [ed.], *Ocean Optics XII*. SPIE.
- ZIBORDI, G., AND G. M. FERRARI. 1995. Instrument self-shading in underwater optical measurements: Experimental data. *Appl. Optics* **34**: 2750–2754.

*Received: 2 October 2007*

*Accepted: 12 April 2008*

*Amended: 28 April 2008*